Electromagnetic Formation Flight for Sparse Aperture Arrays

Daniel W. Kwon*, David W. Miller†, and Raymond J. Sedwick‡
Massachusetts Institute of Technology, Cambridge, MA 02139

Traditional methods of actuating spacecraft in sparse aperture arrays use propellant as a reaction mass. For formation flying systems, propellant becomes a critical consumable which can be quickly exhausted while maintaining relative orientation. Additional problems posed by propellant include optical contamination, plume impingement, thermal emission, and vibration excitation. For these missions where control of relative degrees of freedom is important, we consider using a system of electromagnets, in concert with reaction wheels, to replace the consumables. Electromagnetic Formation Flight sparse apertures, powered by solar energy, are designed differently from traditional propulsion systems, which are based on ΔV. This paper investigates the design of sparse apertures both inside and outside the Earth's gravity field.

I. Introduction

Multi-aperture systems are an emerging concept over traditional monolithic apertures, which are limited by launch vehicle constraints, technology, and cost. By formation flying multi-aperture space-based telescopes and Earth observing satellites, a greater amount of resolution can be achieved with increasing aperture separation. Sparse aperture systems generally use the array rotation as a method of filling the u-v plane for interferometric image construction. The propellant needed for array rotation is dependant on ΔV, which requires propellant mass to increase exponentially according to the rocket equation. One of the limitations of formation flight sparse apertures is the propellant required for formation control. Since propellant is a consumable, the mission lifetime for a spacecraft is limited by the amount of propellant available. Once it is consumed, the spacecraft is rendered useless and its mission is over. Another problematic effect of propellant based systems is impingement of thruster plumes on neighboring spacecraft. Plume impingement can contaminate precision optical surfaces, create unnecessary vibration excitation, produce inadvertent charging, and ablate material off a spacecraft surface. In addition, missions imaging in the infrared spectrum could be thermally blinded or obscured by propellant plumes crossing its field of view[1]. Upon further inspection of sparse aperture arrays, it is the maintenance of relative formation control that is important and most costly.

The alternative to using propellant for actuation of sparse aperture arrays is for each spacecraft to produce their own field that others in the formation can react against. This technique can be achieved by creating a steerable magnetic dipole and is called Electromagnetic Formation Flight (EMFF). EMFF can be implemented on a spacecraft by driving current through three orthogonal electromagnetic coils to create a steerable magnetic dipole in three dimensions. These coils are powered by solar energy, a limitless resource, making the mission lifetime that is dependant on formation control theoretically unbounded. Momentum conservation prohibits control of the motion of the center of mass of the formation using EMFF since only internal forces are present. However, EMFF, in concert with reaction wheels, can be used to control the relative separation, relative attitude and inertial rotation, which are the critical maneuvers for sparse aperture arrays. This paper investigates the maintenance of sparse aperture arrays using non-Keplerian orbits in the Earth's gravitational field. The Terrestrial Planet Finder is used as a focus application outside the Earth's gravitational field.

---

* Graduate Research Assistant, Department of Aeronautics and Astronautics, Room 37-344a, 77 Massachusetts Avenue, Student Member AIAA.
† Associate Professor, Department of Aeronautics and Astronautics, Room 37-327, 77 Massachusetts Avenue, Senior Member AIAA.
‡ Principal Research Scientist, Department of Aeronautics and Astronautics, Room 37-431, 77 Massachusetts Avenue, Senior Member AIAA.

II. Electromagnetic Formation Flight Dynamics

An introduction of the electromagnetic dynamics is helpful before designing EMFF sparse apertures. The simplest method of modeling the forces and torques created by EMFF satellites is to approximate the coils as permanent bar magnets. This is called the far field model and is applicable at distances far enough from the satellite that the electromagnetic coils appear as dipoles. At this distance, the dipole field structure for permanent bar magnets and electromagnetic dipoles are the same. Using the far field model, we can imagine two orthogonal coils represented by a pair of magnets, which have the ability to turn their fields on or off, located in a two dimensional plane as seen in Figure 1.

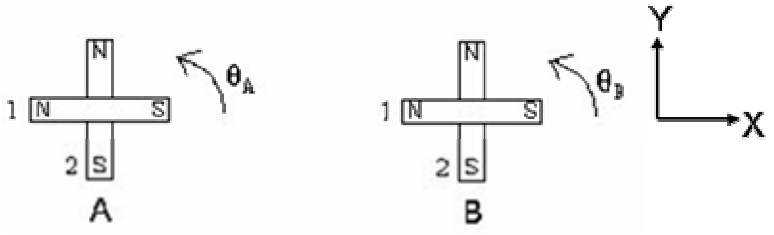

Figure 1. Far field magnetic model.

To create an attractive force, magnet one from both vehicle A and B is turned on, at which point the south or minus polarity from A is attracted to the north or plus polarity of B. The north of A is also repelled from the north of B and the south repelled from the south of B. However, the attractive component of force is much stronger resulting in a net attraction and movement along the x-axis. To create a net repulsive force, the polarity of one of the magnets is reversed. Movement in the y-direction is achieved when the magnetic field generated by one vehicle is orthogonal to the field generated by the other vehicle. For example, by enabling only magnet two on A and magnet one on B while all others are turned off. In this case the plus polarities repel each other causing the magnets to turn in the counter-clockwise direction. In addition the minus polarities repel although this effect is weaker and in the opposite direction. The net effect is a counter-clockwise torque seen on both A and B plus a shear force in the positive y-direction on A and a shear force in the negative y-direction on B. By using a reaction wheel to provide a torque in the clockwise direction, a net shearing motion can be created while maintaining constant angle.

The permanent magnet model works well to understand the various degrees of freedom. EMFF is implemented in three dimensions by using three orthogonal electromagnetic coils which act as dipole vector components and allow a magnetic dipole to be created in any direction by varying the current through the coils. A reaction wheel assembly with three orthogonal wheels is also necessary to provide the counter torques for attitude maintenance.

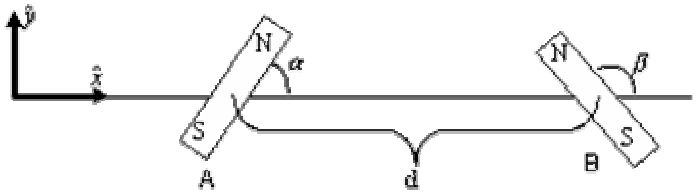

Figure 2. Two dipoles interacting in the far field.

The interaction force between two arbitrary loops of current can be determined by the Law of Biot and Savart. However, they are difficult to solve except for cases of special symmetry such as circular coils. Therefore circular EMFF coils have been assumed for all analyses. The full three dimensional set of equations for forces and torques in the far field have been developed by Sedwick[2]. A simplified two dimensional set for two electromagnetic dipoles separated by a distance, *d*, oriented at arbitrary angles as seen in Figure 2 is given for the left dipole as

$$
\begin{aligned}
F_x &= \frac{3}{4\pi}\frac{\mu_0 \mu_A \mu_B}{d^4}(2\cos\alpha\cos\beta - \sin\alpha\sin\beta) \\
F_y &= -\frac{3}{4\pi}\frac{\mu_0 \mu_A \mu_B}{d^4}(\cos\alpha\sin\beta + \sin\alpha\cos\beta) \\
T_z &= -\frac{1}{4\pi}\frac{\mu_0 \mu_A \mu_B}{d^3}(\cos\alpha\sin\beta + 2\sin\alpha\cos\beta)
\end{aligned}
\tag{1}
$$

The magnetic moment, μ, is defined as a function of the number of loops in a coil, n, the current in the conductor, i, and the coil radius, R_c, in the equation

$$\mu = ni\pi R_c^2 \tag{2}$$

If the dipole orientation angles are set to zero ($\alpha = \beta = 0$), the two dipoles align and the forces and torque simplify to

$$\begin{aligned} F_x &= \frac{3}{2\pi}\mu_o \frac{\mu_A \mu_B}{d^4} \\ F_y &= 0 \\ T_z &= 0 \end{aligned} \tag{3}$$

In order to generate large magnetic dipoles, Eq. (2) indicates that a favorable electromagnetic coil design is one with many turns and high current. However, this drives up electromagnetic coil and solar array masses. Conventional coil conductors such as copper suffer from such high current application, since resistance causes significant heat generation and power losses. Therefore the design should utilize a coil that has the lowest resistance possible.

Superconducting material has zero resistance when cooled below a critical temperature resulting in no thermal heating and no power losses across the wire. With high temperature superconducting (HTS) wire, an electromagnet could be built to any size needed. Since there is no resistance, there is no heat production and a coil of any cross-sectional area can be made without fear of overheating the wire. Zero-resistance also means no power is required to maintain a high current through the wire causing the mass of the solar array to be determined by the power requirements of the spacecraft bus and payload mass, and not the coil. The only losses are in the power subsystem itself such as from regulators, switches, and batteries. Therefore the only limitation on the current is the critical current density of the superconducting wire.

There is a critical current density in the conductor above which the HTS will no longer conduct current at zero resistance. This clearly sets a limit on dipole strength. Furthermore, adding more coil will allow the dipole strength to be increased but at the cost of mass. As a result, the current limit and effect of HTS conductor mass density can be modeled.

$$\begin{aligned} i &= I_c A_c \\ M_c &= 2n\pi R_c A_c \rho_c \end{aligned} \tag{4}$$

where I_c is the critical current density (Amps/m^2), A_c is the cross-sectional area of the HTS wire, M_c is the mass of the coil, and ρ_c is the volumetric mass density of the HTS wire. Substituting Eqs. (4) and (2) into Eq. (3), gives Eq. (5) which can be further simplified if the coils on the two vehicles are assumed to be identical.

$$F_x = \frac{3}{8\pi}\mu_o \left(\frac{I_c}{\rho_c}\right)^2 M_{c_A} R_{c_A} M_{c_B} R_{c_B} \frac{1}{d^4} = \frac{3}{8\pi}\mu_o \left(\frac{I_c}{\rho_c}\right)^2 \left(M_c R_c\right)^2 \frac{1}{d^4} \tag{5}$$

There are three main design parameters in Eq. (5). The I_c/ρ_c quantity is the HTS technology parameter and is fixed for various types of HTS wire. With better HTS technology, either through higher current density or lower mass density wires, this technology factor can be improved. The I_c/ρ_c has a value of 16,250 A·m/kg for current state of the art high strength HTS wire at 77 degrees Kelvin[3]. The critical current density increases by a factor of six if the wire is maintained at 20 degrees Kelvin. The M_cR_c quantity is the coil design parameter which can vary according to the design of a spacecraft. Finally, the array design parameter sets the separation distance, d. This is the design parameter most sensitive to changes since it has a fourth power relationship. These three design parameters will be used throughout the chapter to understand how design affects the overall EMFF system. Eq. (5) can be used to understand the amount of force EMFF can generate using two identical spacecraft. Figure 3 shows the axial force versus separation distance for state of the art HTS technology as well as a factor of three improvement in I_c/ρ_c. Curves are shown for different coil designs (M_cR_c). For example, if two 300 kg satellites with one meter radius coils need 10 mN of thrust and 30 kg is dedicated to the coil on each satellite, this force can be achieved using state of the

art HTS at a separation of 43 m, indicated by the circle in Figure 3a. This same force can be generated at a separation of approximately 77 m using a HTS technology with a three times improvement, indicated by the circle in Figure 3b.

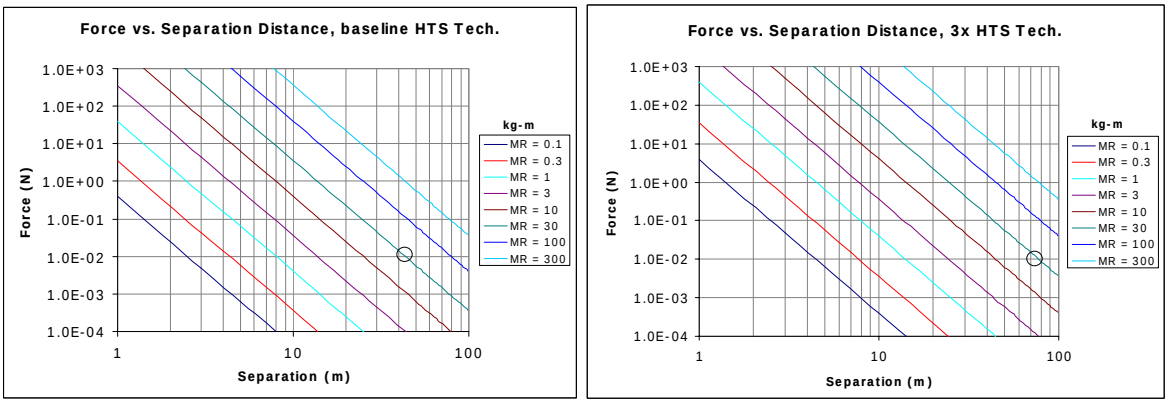

a) b)

Figure 3. Axial force versus separation distance for current HTS technology (a) and a factor of three improvement (b).

III. Summary of Non-Keplerian Orbits

Consider two or more satellites in LEO that are evenly separated in the cross-track direction in order to synthesize a sparse aperture. Figure 4 shows such a scenario. The center satellite is in a ninety minute period, circular orbit. The outer two satellites are in non-Keplerian orbits and therefore must be constantly accelerated in order to keep them in this geometry. This is an example of the need to fight persistent gravitational accelerations in order to maintain a cluster of Earth-orbiting satellites. While it has been shown that it is easier to let the geometry be dynamic[4], the problem solved here is meant to show the relative capabilities of EMFF and micropropulsion systems. It is reasonable to assume that such a comparison will hold true for other formations as well.

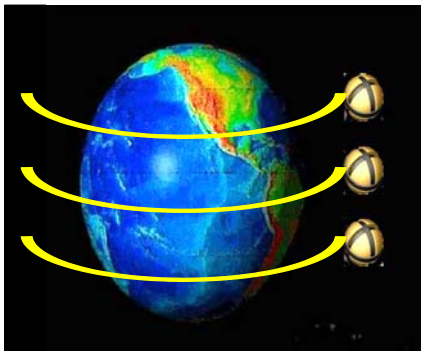

Figure 4. Cross-track distribution of satellites in LEO.

To better understand the requirements imposed on these spacecraft, consider Hill's equations governing relative motion between satellites in a gravity well,

$$\begin{aligned} \ddot{x} - 3n^2 x - 2n\dot{y} &= a_x \\ \ddot{y} + 2n\dot{x} &= a_y \\ \ddot{z} + n^2 z &= a_z \end{aligned} \tag{6}$$

where x is in the zenith direction, y is in the orbital velocity direction and z is in the cross-track direction for a right-handed coordinate frame. Therefore, the offsets of the two outer satellites are in the z direction and an acceleration of

$$a_z = n^2 z \tag{7}$$

is required to maintain them at those offsets.

A. Maintaining Cross-Track Offset Using Thrust

Now, consider the use of thrust to provide this constant acceleration. Then compare this result with that using EMFF. Using thrusters, the rocket equation is needed to relate propellant mass to ΔV and mission lifetime,

$$m_p = m_f \left(e^{\frac{\Delta V}{I_{sp} g}} - 1 \right) = \left(m_o + m_{sa} \right) \left(e^{\frac{n^2 z T}{I_{sp} g}} - 1 \right) \tag{8}$$

where I_{sp} is the specific impulse and g is the acceleration due to Earth's gravity at sea level, and T is the mission lifetime. The masses m_p, m_o, and m_{sa} correspond to the propellant, the core vehicle, and the solar array, respectively. The solar array is sized to provide the power needed to generate the thrust

$$\eta P = \frac{1}{2} \tau I_{sp} g \tag{9}$$

where τ is the thrust, η is the power conversion efficiency, and P is the power. Notice that higher I_{sp} systems require more power in order to generate the same thrust. This, in turn, requires larger and more massive solar arrays thereby reducing the net acceleration of high I_{sp} systems (I_{sp} > 3000 seconds). The result is that there exists an optimum I_{sp} based upon the specific power of the solar array (i.e., Watts per kilogram). Combining Eqs. (7), (8), and (9) gives the acceleration and the total mass of the satellite, m_T,

$$\begin{aligned} \frac{\tau}{m_T} = a_z \qquad &\Rightarrow \qquad \frac{\frac{2\eta P}{I_{sp} g}}{\left(m_o + \frac{P}{\overline{P}} \right) e^{\frac{n^2 z T}{I_{sp} g}}} = n^2 z \\ m_T = m_o + m_p + m_{sa} \qquad &\Rightarrow \qquad m_T = \left(m_o + \frac{P}{\overline{P}} \right) e^{\frac{n^2 z T}{I_{sp} g}} \end{aligned} \tag{10}$$

where $\overline{P}$ is the specific power of the solar array. Solving for the required power and substituting into the mass relationship,

$$m_T = \frac{m_o}{e^{-\frac{n^2 z T}{I_{sp} g}} - n^2 z \frac{I_{sp} g}{2\eta \overline{P}}} \tag{11}$$

reveals that there is a cross-track offset beyond which thrust cannot provide the required acceleration.

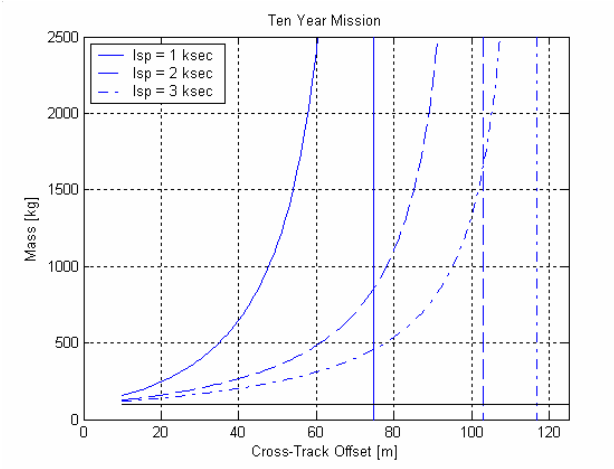

Figure 5. Total mass versus cross-track offset for ten year mission.

Figure 5 shows the total satellite mass as a function of the offset position in the cross-track direction for different values of I_{sp}. The horizontal black line denotes the core mass of the satellite. Note that the actual separation between the two satellites is twice the cross-track offset. The orbital period is ninety minutes (n=0.0011636 rad/sec), the power conversion efficiency is 0.5 (50%), the core mass is 100 kg, and the specific power of the solar array is 25 Watts/kg. A ten year mission is assumed since typical mission design is for five year reliability and ten years of consumables. The maximum cross-track offset that can be supported by micropropulsion systems can also be seen in Figure 5. The vertical line, in each curve corresponding to a specific I_{sp}, reveals the cross-track offset where the satellite mass becomes infinite.

B. Maintaining Cross-Track Offset Using EMFF

Now consider the use of EMFF to maintain the cross-track offset. Using Eq. (5) for the thrust generated by two identical EMFF satellites, the acceleration and mass are given by,

$$\frac{\tau}{m_T} = n^2 z \qquad \Rightarrow \qquad \frac{\frac{3}{8\pi}\mu_o \left(\frac{I_c}{\rho_c}\right)^2 \left(M_c R_c\right)^2 \frac{1}{\left(2z\right)^4}}{m_o + \frac{I_c^2 R + P_T}{\bar{P}} + M_c} = n^2 z \tag{12}$$

$$m_T = m_o + m_{sa} + M_c \qquad \Rightarrow \qquad m_T = m_o + \frac{I_c^2 R + P_T}{\bar{P}} + M_c$$

where R is the current amplifier resistance (10 milli-Ohms) and P_T is the cryo-cooler power needed to keep the coils at 77 degrees Kelvin (100 Watts). Figure 6 plots the total satellite mass versus offset position for currently available HTS, threefold, and tenfold improvement in the technology in red. Also plotted are the curves for thrusters in blue. Notice that 3000 second I_{sp} is more mass efficient than EMFF, using currently available technology, beyond a forty meter offset.

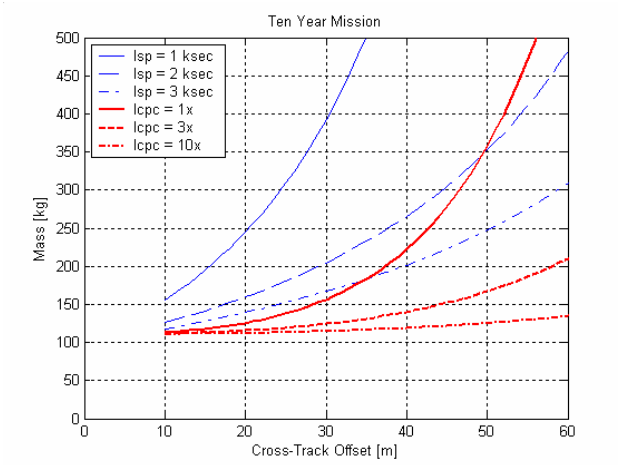

Figure 6. Comparison of two satellites maintaining a variety of cross-track separations using thrusters and EMFF.

Several of the key benefits of EMFF over thrusters are as follows. First, EMFF does not have a mission lifetime limitation. Second, adding an additional satellite improves performance whereas it does not affect the thruster-based performance. Every time we add an extra, identical satellite and evenly distribute these satellites in the cross-track direction, the resulting reduction in neighbor-to-neighbor separation dramatically increases the force between neighbors. Notice the change in the numerator (force term) from Eq. (12) to Eq. (13). The force on the outermost satellite is due to the sum of forces from all of the other satellites. When a third satellite is added to a two satellite cluster, the neighbor-to-neighbor separation is divided in half and the neighbor-to-neighbor force increases by a factor of sixteen (2^4).

$$\frac{\tau}{m_T} = n^2 z \qquad \Rightarrow \qquad \frac{\frac{3}{8\pi}\mu_o \left(\frac{I_c}{\rho_c}\right)^2 \left(M_c R_c\right)^2 \sum_{j=1}^{n_{S/C}-1} \left(\frac{n_{S/C}-1}{2jz}\right)^4}{m_o + \frac{I_c^2 R + P_T}{\bar{P}} + M_c} = n^2 z \tag{13}$$

$$m_T = m_o + m_{sa} + M_c \qquad \Rightarrow \qquad m_T = m_o + \frac{I_c^2 R + P_T}{\bar{P}} + M_c$$

Figure 7 provides a comparison between thrusters and EMFF for two and more satellites. An I_{sp} of 3000 seconds is assumed for the thruster-based system. Notice the vertical dash-dot line which corresponds to the maximum cross-track offset that that thruster can support. The EMFF satellites are equipped with HTS that has an I_c/ρ_c that is three (Figure 7a) and ten (Figure 7b) times that which is currently available. Notice that the achievable cross-track offset is dramatically increased when more satellites are used. The addition of extra satellites does not help the thruster-based system. With a tenfold increase in HTS technology, four 2.0 meter diameter, 100 kg core mass satellites (230 kg total) can be continuously held evenly distributed in a cross-track line that is half a kilometer in length for an indefinite amount of time. This can even be improved further by not requiring the satellites to be identical. Instead, the further the offset, the smaller the satellite.

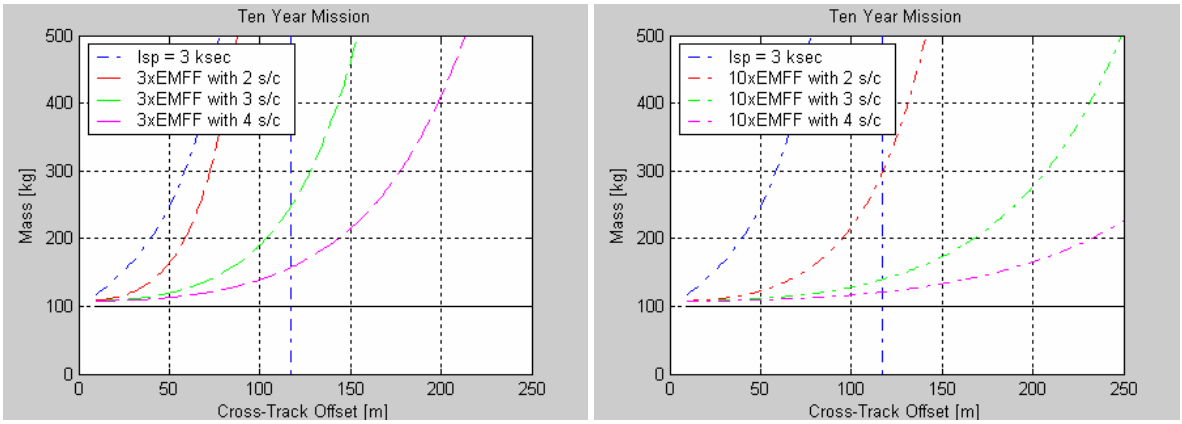

a) b)

Figure 7. Cross-track separation comparison of 3000 second I_{sp} to threefold (a) and tenfold (b) HTS improvement implemented on 2, 3, and 4 evenly distributed satellites.

The boundary between when it is more mass-effective to use 3000 second I_{sp} thrusters versus EMFF is indicated in Figure 8a. The horizontal axis is cross-track offset while the vertical axis is orbital period. The three curves correspond to the technology level of the HTS. Three regions of interest exist. To the bottom right, the power needed to generate the requisite thrust is unavailable and EMFF is the only option. The region above the colored curves, and above the thruster limit line, corresponds to cross-track offsets and orbital periods where thrusters are more mass-effective. The region below the colored curves but above the thruster limit line corresponds to offsets and periods where EMFF is more mass effective. Given an EMFF technology level, there is a specific cross-track offset for which EMFF is well tuned. In Figure 8a, that offset ranges from 20 to 70 meters depending upon the technology level.

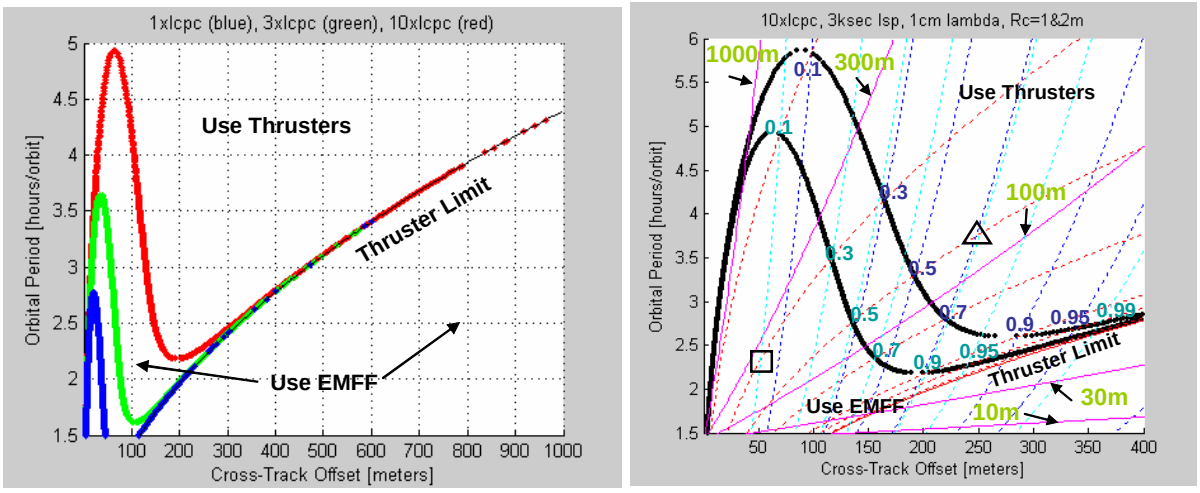

a) b)

Figure 8. Equal mass contours for I_{sp}=3000 thrusters and EMFF with various HTS technology (a) and with various coil radii and contours of constant ground resolution (b)

Figure 8b is a zoomed in version of Figure 8a as seen by a smaller range for the cross-track offset along the x-axis. There are several things to indicate on this figure. First, two curved mass contours describe an EMFF system with a ten times HTS technology improvement for a one meter (lower contour) and two meter (upper contour) coil radius. Second, the diagonal magenta lines indicate constant ground resolution accomplished by the sparse aperture array. Third, constant mass fractions are also plotted for thrusters (red), one meter EMFF coil radius (teal), and two meter EMFF coil radius (blue) systems. The mass fraction value is labeled near each line. The best way to understand how to use Figure 8b is by example. The triangle in the figure is a sparse aperture system with a ground resolution close to 100 meters. To achieve this design, one can either select a system with 50% of its mass allocated

to thrusters, a system with 70% of its mass allocated to EMFF using a two meter radius coil, a system with 90% of its mass allocated to EMFF using a one meter radius coil. Naturally, the thruster system is more favorable. Similar results to this example are found in the area marked 'Use Thrusters.' A second example is indicated by the square in Figure 8b, which indicates a design that yields a ground resolution close to 300 m. This can be achieved with a system with 30% of its mass allocated to thrusters or a system with 10% of its mass allocated to EMFF with two meter radius coils. In this example, the EMFF system is more favorable and similarly in the area marked 'Use EMFF' consists of similar design scenarios. Figure 8b also shows that increasing the radius of the coil opens the range over which EMFF is favored over thrusters.

An alternative method of illustrating the information in Figure 8b can be seen in Figure 9, which plots the average mission acceleration necessary for a sparse aperture array to maintain a certain cross-track offset in LEO. Shown are the mass contours and lines of constant mass fraction for a one meter coil radius with baseline HTS technology (blue) and three fold improvement in HTS technology (teal). Each satellite has a nominal mass of 150 kg and the mission lifetime is ten years. The EMFF system is more mass efficient that the 3000 second I_{sp} thrusters at providing close proximity acceleration.

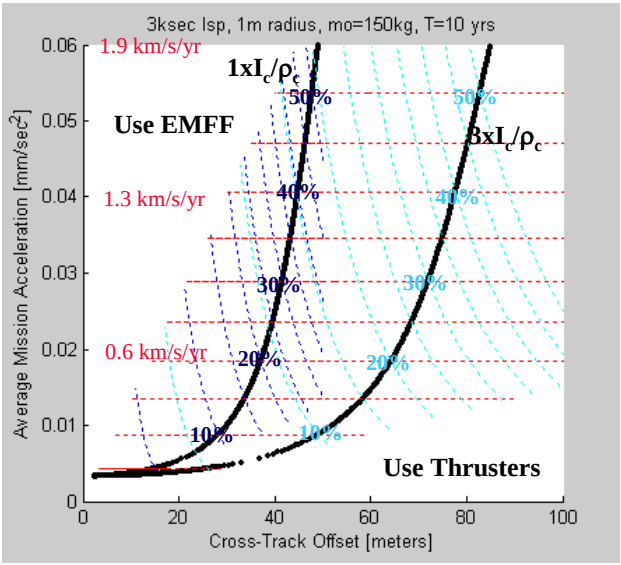

Figure 9. Thruster and EMFF favored regimes with average mission acceleration.

IV. Application to Terrestrial Planet Finder

The cornerstone mission of NASA's Origins program is the Terrestrial Planet Finder (TPF). A possible design for the mission is a four-aperture Michelson interferometer with a resolution capable of viewing extra-solar planets. The entire system consists of five spacecraft, where the center spacecraft is a combiner. One possible configuration is a collinear array shown in Figure 10, with each aperture (collector spacecraft) at equal separation distances and with the combiner in the center of the array. In order to detect planets, the array must rotate to fill the Fourier (u-v) plane. Current TPF designs use high I_{sp} thrusters on each spacecraft for this purpose. The faster the array rotation, the more images it can collect, and the more science that can be conducted (assuming that the interferometer maintains the necessary signal to noise ratio to achieve images). Unfortunately, increasing the rotation rate puts a greater demand on the propulsion system and more propellant must be expended. Consumables are then a limiting factor on the mission duration and the consequently the science returns for TPF.

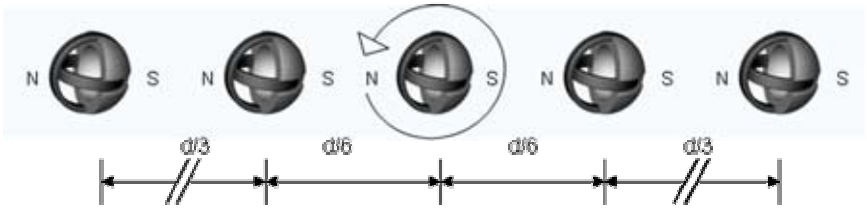

Figure 10. Five Spacecraft TPF Design using EMFF.

The goal of this section is to develop a model for TPF using both EMFF and high I_{sp} micropropulsion systems and to show how they trade with mass as a metric for a variety of mission parameters such as lifetime, baseline, and rotation rate. To create a convincing trade, it is not sufficient enough to only compare the propulsion mass versus the EMFF coil mass, since the different propulsive options are closely coupled with other subsystems such as the attitude control subsystem (ACS), power, and structures. Therefore, the HTS coil, the main "propulsive" component for EMFF, is modeled with its associated thermal, power, structural, and ACS components. Determining how the EMFF and micropropulsion systems affect the total mass of the array is useful for future designs of TPF.

The starting point for the model consists of mass and inertia data for a collector spacecraft designed by the Jet Propulsion Laboratory (JPL)[5]. The subsystems common to both the JPL model and the EMFF and micropropulsion models are shown in Table 1. These common subsystems consist of the entire collector payload and most of the collector spacecraft subsystems and form the core dry mass, m_{dry}, for both the EMFF and micropropulsion models.

Table 1. Subsystems used in JPL, EMFF, and micropropulsion system models.

	Subsystem	**Mass, JPL model [kg]**	**Symbol, EMFF system**	**Symbol, Micropropulsion systems**
Common Subsystems	Collector Payload	707.12	N/A	N/A
	Collector Spacecraft	695.27	N/A	N/A
Common Subsystems Total		**1402.39**	m_{dry}	m_{dry}
Different Subsystems	Reaction Control Subsystem	156.56	m_{coil}	$m_{propulsion}$, $m_{propellant}$
	Attitude Control (single Reaction Wheel)	5.96	m_{RW}	m_{RW}
	Power (Solar Arrays)	57.56	m_{power}	m_{SA}
	Thermal	0	$m_{thermal}$	N/A
	Structure	0	$m_{structure}$	Included in $m_{propulsion}$
Different Subsystems Total		**220.08**	m_{EMFF}	$m_{PropSys}$
TOTAL SPACECRAFT		**1622.47**	m_{sc}	m_{sc}

The subsystems that are different from both the JPL model and the EMFF and micropropulsion models are also shown in Table 1 under the section called 'Different Subsystems.' The symbolic masses denoted in Table 1 are discussed in this section. There are three subsystems from the JPL model that are modeled differently by the EMFF and micropropulsion systems and consequently have differing masses. First, the Reaction Control Subsystem (RCS) mass (156 kg) on the JPL model is not part of the EMFF RCS mass or micropropulsion RCS mass. Instead, the EMFF RCS mass is denoted by m_{coil} and the micropropulsion RCS masses are denoted by $m_{propulsion}$ and $m_{propellant}$. The second different subsystem is the attitude control subsystem. The EMFF and micropropulsion models do not consist of the entire ACS components (star trackers, inertial reference units, etc.) that are part of the JPL collector spacecraft model. The one component that is different and is determined by the EMFF and micropropulsion systems is the reaction wheel responsible for angular momentum management in the plane of the array rotation. This wheel is denoted by m_{RW}. A single reaction wheel in the JPL model has a mass of 5.96 kg. The third different subsystem is the power subsystem, which is denoted by m_{power} in the EMFF model and m_{SA} in the micropropulsion models. The power subsystem mass for both EMFF micropropulsion systems consists of both the solar arrays and power processing units.

There are two subsystems that are part of the EMFF model that do not exist on the JPL or micropropulsion models. The first is the EMFF thermal control subsystem, denoted by $m_{thermal}$. The second is the structural mass needed by the RCS subsystem, which is denoted by $m_{structure}$ for the EMFF system. The structural mass needed by the micropropulsion systems' RCS is already included in $m_{propulsion}$.

A few assumptions have been made about the TPF system. No detailed combiner mass exists yet, so it is assumed that the combiner has the same mass as the collector. The thermal control system currently allocated on the collector payload will only be used for the optics subsystem. For this reason the cryogenic thermal control system for the EMFF coils will be designed separately. It could be feasible for future designs to combine the two thermal control subsystems for possible mass and power savings. The rotation rate for TPF is assumed to be target-independent, and therefore constant. A nominal rotation rate of four hours per revolution is assumed, however, this mission parameter will be varied to determine how the spin rate affects the TPF design.

In summary, the JPL model and the EMFF and micropropulsion models share common subsystems, which have a total mass of 1402.39 kg. The total EMFF system mass is

$$m_{EMFF} = m_{coil} + m_{RW} + m_{power} + m_{thermal} + m_{structure} \tag{14}$$

Combining the EMFF system mass with the dry mass results in the mass for an entire EMFF spacecraft

$$m_{sc} = m_{EMFF} + m_{dry} \tag{15}$$

Similarly, the total micropropulsion system mass is determined by

$$m_{PropSys} = m_{propulsion} + m_{propellant} + m_{RW} + m_{SA} \tag{16}$$

Combining the micropropulsion system mass with the dry mass results in the mass for an entire micropropulsion spacecraft

$$m_{sc} = m_{PropSys} + m_{dry} \tag{17}$$

The detailed designs to determine m_{EMFF} and $m_{PropSys}$ can be found by Reichbach and Kwon[6]. The following two sections provide a high level summary of the EMFF and micropropulsion models.

C. EMFF TPF Model

As seen in Eq. (14), the EMFF related subsystems consist of the HTS coil, reaction wheel, power subsystem, cryogenic thermal subsystem, and structures. Since TPF is spinning during observations, the array must be "spun up" from relative rest to the desired angular rate. For the array to spin about the center spacecraft, each collector spacecraft revolves around the combiner while also rotating about their respective body centers at that rate to keep the desired spacecraft face pointing towards the combiner. For the EMFF system, the reaction wheel and electromagnets are used to initiate both the rotation of each spacecraft and the array revolution in addition to providing the necessary centripetal force to maintain the revolution of the array. To determine the mass of the coils, the force generated by the coils must be equal to the centripetal force of the array during rotation. Applying Eq. (5) to an array of five spacecraft yields

$$F = \frac{3}{8\pi}\mu_o\left(\frac{I_c}{\rho_c}\right)^2\left(M_c R_c\right)^2\frac{1649}{16d^4} = m_{tot}\omega^2\frac{d}{2} \tag{18}$$

where the 1649/16 factor results from the bridging of fields by all the spacecraft in the array. It is assumed that the EMFF coils on all five spacecraft are identical. This enables the collector spacecraft to reconfigure to different positions in the array if necessary.

The thermal subsystem consists of a cryogenic cooler to keep the HTS coil at superconducting temperatures. The beams necessary to attach the three orthogonal coils to the spacecraft bus make up the structures subsystem mass. The total EMFF power budget consists of the power for the spacecraft bus, coils, thermal subsystem, and reaction wheel

$$P_{total} = P_{bus} + P_{coils} + P_{thermal} + P_{RW} \tag{19}$$

Once the total power is determined, the mass of the solar arrays can be found. The solar array mass and the coil power processing unit mass consist of the power subsystem mass.

A breakdown of the EMFF system mass for a four hour rotation, 75 m baseline, and ten year mission lifetime for the three levels of HTS technology are shown in Figure 11. There are several observations that can be made from these results. First, the total EMFF system mass for the baseline technology is less than the mass of the JPL RCS (156.56 kg). Second, as HTS technology increases, the overall EMFF system mass decreases, most significantly at the three fold HTS technology improvement level. Third, no subsystem noticeably dominates the overall EMFF

mass at baseline HTS technology; however the reaction wheel consists of most of the total mass fraction for higher HTS technology levels. This is because the coil and power masses are becoming much smaller, and not because the reaction wheel is becoming larger. It should also be noted that the structures and thermal subsystem masses are constant for all designs.

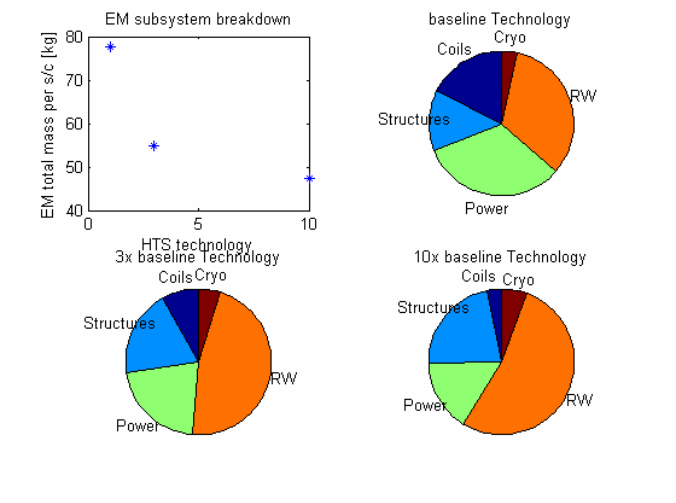

Figure 11. EMFF Subsystem mass breakdown: four hour rotation, 75 m baseline.

D. Micropropulsion Model

The micropropulsion systems modeled are pulse plasma thrusters (PPTs) and colloids. In order for TPF to rotate, propellant must constantly be expended by the collector spacecraft in order to achieve the centripetal force necessary for a steady state spin. The centripetal force for the outer collector spacecraft is given by

$$F_c = \frac{d}{2} m_{tot} \omega^2 \tag{20}$$

where ω is the steady state rotation rate, and m_{tot} is the total spacecraft mass (wet and dry mass). Using Eq. (20) the ΔV necessary for station keeping the outer collector spacecraft is

$$\Delta V_{rotation} = \frac{d}{2} \omega^2 T \tag{21}$$

where T is the duration of the rotation. The ΔV for the inner collector spacecraft follows the same form as Eq. (21) but is a factor of three less, since the distance to the combiner is less, as shown in Figure 10. There is no propulsion system necessary on the combiner since it only needs to spin in place. In addition, the ΔV budget accounts for array slewing, non-observation time (i.e. time spent not rotating), and thrusters firing off-axis for plume impingement avoidance. Once the total ΔV is calculated, the propellant mass can be determined.

The propulsion dry mass, $m_{propulsion}$, consists of the necessary structures, tanks and tubing, electronics, and power processing units needed by PPTs and colloids. Since the exact designs for the JPL RCS are unknown, trades between the JPL RCS mass and the micropropulsion system mass are not comparable.

E. TPF System Trades

The results of the EMFF and micropropulsion models for an four hour rotation and 75 m baseline TPF mission are seen in Figure 12a, which plots the total mass of all five spacecraft as a function of mission lifetime. The thin solid horizontal black line at approximately 7012 kg represents the total dry mass of all five spacecraft. This is the mass of the system without a propulsion system, reaction wheel for array spin-up, and solar arrays. The thick solid horizontal black line at 8112 kg represents the total JPL design mass. Any system above this line for any duration mission represents an option that is not mass favorable when compared to the current JPL design and is not considered favorable. The PPTs systems and colloids systems (less than 8.5 years) are less massive than the current JPL design, but the EMFF system using current state of the art HTS technology is more favorable than either of

them for missions longer than a few years when considering mass. In addition to the trade with the micropropulsion models, an important observation is that EMFF system trades favorably compared to the JPL model. Higher HTS technology can decrease the overall EMFF system to make it even more favorable in terms of mass. Since the EMFF system has no consumables its mission can last beyond ten years.

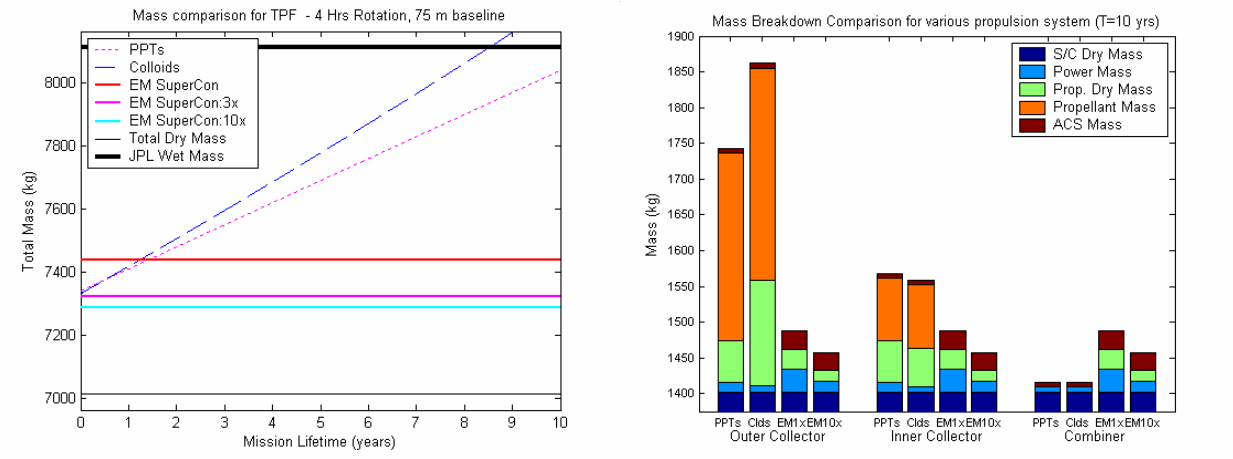

a) b)

Figure 12. Mass comparison (a) and mass breakdown (b) for TPF using various propulsion systems, four hr. rotation, 75 m baseline.

The mass breakdown for the outer collector, inner collector and combiner spacecraft for the various systems are shown in Figure 12b. Note that for the propellant-based options, the outer collector is the most massive since it has the highest centripetal load, while the combiner does not have any propulsion mass since it only needs to rotate in place. The propellant-based options also have a relatively high amount of mass (excluding the dry mass) allocated for propellant. If the micropropulsion systems consisted of a combiner with a propulsion system (which is likely in reality), their overall mass will increase beyond that seen in Figure 12a and Figure 12b.

The effect of designing for different baselines and rotation rates is shown in Figure 13 for PPTs and EMFF using three times HTS technology level with a ten year mission lifetime. When comparing designs of different rotation rates, some PPT designs are less massive than EMFF designs, however these only exist for PPTs with slower rotation rates than EMFF. EMFF is more mass favorable than PPTs for all baselines when considering the same rotation rate. For large baseline systems and fast rotation rates, the EMFF TPF design is well below the JPL model.

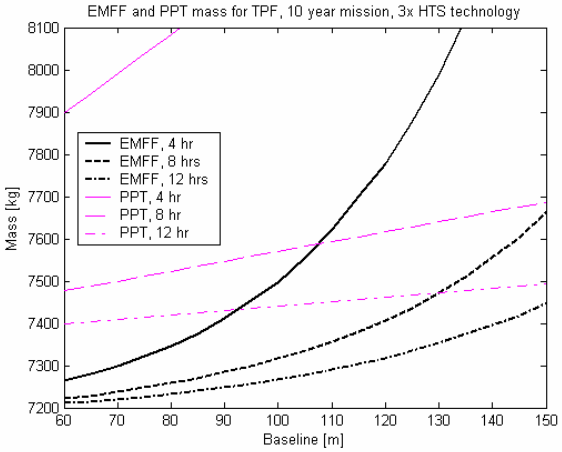

Figure 13. EMFF (3x HTS technology) and PPT mass versus baseline for various rotation rates.

V. Conclusions

This paper has presented electromagnetic formation flight dynamics and applied them to sparse aperture arrays. In the Earth's gravitational field EMFF and thrusters were used to form non-Keplerian orbits. Mass contour plots were used to understand how EMFF and thrusters traded for various ground resolutions, EMFF coil sizes, HTS

technology levels, and average mission accelerations. Several scenarios existed where EMFF was a more favorable mass option than high I_{sp} micropropulsion thrusters. Using EMFF for close proximity accelerations and close proximity cross-track separations are two examples of these.

EMFF was also a feasible option for sparse aperture arrays outside of the Earth's gravitational field, such as NASA's Terrestrial Planet Finder. Electromagnets were used to provide the centripetal acceleration necessary for array rotation. Furthermore, it did so with subsystem requirements and mass fractions that were quite favorable when compared to thrusters. When compared to high I_{sp} propellant-based systems, the EMFF design was deemed to be the most attractive option especially when long mission lifetimes were considered. The lack of propellant contamination and reliance on consumables further reinforces the viability of this EMFF concept.

In theory, the proposed EMFF sparse aperture arrays can operate indefinitely or at least until component failure, since no non-renewable resources (propellant) are used. System trades, as well as controllability studies and experimental validation must be performed to further understand the capabilities of electromagnetic formation flight sparse aperture arrays.

Acknowledgments

The authors would like to thank the Lockheed Martin Advanced Technology Center and NASA Jet Propulsion Laboratory for support of this research effort.

References

[1]Reichbach, J., Sedwick, R. J., and Martinez-Sanchez, M., "Micropropulsion System Selection for Precision Formation Flying Satellites," Space Engineering Research Center, Rept. 1-01, Massachusetts Inst. of Technology, Cambridge, MA, Jan. 2001.

[2]Sedwick, R. J., and Schweighart, S. A., "Propellantless Spin-Up and Reorientation of Tethered or Electromagnetically Coupled Spacecraft," Society of Photo-Optical Instrumentation Engineers Highly Innovative Space Telescope Concepts Conf., Paper SPIE 4849-26, Aug. 2002.

[3]American superconductor, "Bi-2223 High Strength Wire," URL: http://www.amsuper.com/products/htsWire/index.html [cited 2 February 2003].

4 Schweighart, S. A., and Sedwick, R. J., "High-Fidelity Linearized J2 Model for Satellite Formation Flying," Journal of Guidance Control, and Dynamics, Vol. 25, No. 5, 2002, pp. 1073–1080.

[5]Beda, Michael G., *Structural Analysis Summary Collector Spacecraft* Presentation, Jet Propulsion Laboratory, June 11, 2004.

[6]Kwon, Daniel W, and Miller, David W., "Electromagnetic Formation Flight System Designs: Application to Terrestrial Planet Finder," Masters Thesis, Massachusetts Inst. of Technology, Cambridge, MA, Sept. 2004.